International Journal of Nanomedicine

Dovepress
open access to scientific and medical research

Open Access Full Text Article

ORIGINAL RESEARCH

SMARCB1 Gene Therapy Using a Novel Tumor-Targeted Nanomedicine Enhances Anti-Cancer Efficacy in a Mouse Model of Atypical Teratoid Rhabdoid Tumors

Sang-Soo Kim[1,2], Manish Moghe[1], Antonina Rait[1], Kathryn Donaldson[1], Joe B Harford[2], Esther H Chang[1]

[1]Department of Oncology, Lombardi Comprehensive Cancer Center, Georgetown University Medical Center, Washington, DC, USA; [2]SynerGene Therapeutics, Inc, Potomac, MD, USA

Correspondence: Esther H Chang, Lombardi Comprehensive Cancer Center, Georgetown University, 3970 Reservoir Road N.W., Research Building E420, Washington, DC, 20057, USA, Email change@georgetown.edu

Purpose: Atypical teratoid rhabdoid tumor (ATRT) is a deadly, fast-growing form of pediatric brain cancer with poor prognosis. Most ATRTs are associated with inactivation of SMARCB1, a subunit of the chromatin remodeling complex, which is involved in developmental processes. The recent identification of SMARCB1 as a tumor suppressor gene suggests that restoration of SMARCB1 could be an effective therapeutic approach.

Methods: We tested SMARCB1 gene therapy in SMARCB1-deficient rhabdoid tumor cells using a novel tumor-targeted nanomedicine (termed scL-SMARCB1) to deliver wild-type SMARCB1. Our nanomedicine is a systemically administered immuno-lipid nanoparticle that can actively cross the blood-brain barrier via transferrin receptor-mediated transcytosis and selectively target tumor cells via transferrin receptor-mediated endocytosis. We studied the antitumor activity of the scL-SMARCB1 nanocomplex either as a single agent or in combination with traditional treatment modalities in preclinical models of SMARCB1-deficient ATRT.

Results: Restoration of SMARCB1 expression by the scL-SMARCB1 nanocomplex blocked proliferation, and induced senescence and apoptosis in ATRT cells. Systemic administration of the scL-SMARCB1 nanocomplex demonstrated antitumor efficacy as monotherapy in mice bearing ATRT xenografts, where the expression of exogenous SMARCB1 modulates MYC-target genes. scL-SMARCB1 demonstrated even greater antitumor efficacy when combined with either cisplatin-based chemotherapy or radiation therapy, resulting in significantly improved survival of ATRT-bearing mice.

Conclusion: Collectively, our data suggest that restoring SMARCB1 function via the scL-SMARCB1 nanocomplex may lead to therapeutic benefits in ATRT patients when combined with traditional chemoradiation therapies.

Keywords: lipid nanoparticle, nanodelivery, SMARCB1, gene therapy, atypical teratoid rhabdoid tumor

Introduction

Brain cancer is one of the leading causes of cancer-associated deaths among children.[1] Current treatment modalities (eg, surgical resection, intensive chemotherapy, and radiation therapy) have shown limited effectiveness. Moreover, current treatment options often cause nonspecific cytotoxic effects that negatively affect the development of the young patient's brain, resulting in long-term neurological deficits. In particular, atypical teratoid rhabdoid tumor (ATRT) is a rare but highly malignant form of brain cancer that predominantly affects children under three years.[2,3] The median age at diagnosis is approximately 17 months, and patients typically survive less than one year after diagnosis.[2,4] Currently, there is no definitive standard of care for ATRT, and traditional treatments are not effective enough to stop aggressive progression of the disease. Given the dismal prognosis associated with ATRT, better treatment approaches are urgently needed to improve the treatment outcomes in these very young patients.

Received: 6 January 2024
Accepted: 11 June 2024
Published: 14 June 2024

© 2024 Kim et al. This work is published and licensed by Dove Medical Press Limited. The full terms of this license are available at https://www.dovepress.com/terms.php and incorporate the Creative Commons Attribution – Non Commercial (unported, v3.0) License (http://creativecommons.org/licenses/by-nc/3.0/). By accessing the work you hereby accept the Terms. Non-commercial uses of the work are permitted without any further permission from Dove Medical Press Limited, provided the work is properly attributed. For permission for commercial use of this work, please see paragraphs 4.2 and 5 of our Terms (https://www.dovepress.com/terms.php).

Graphical Abstract

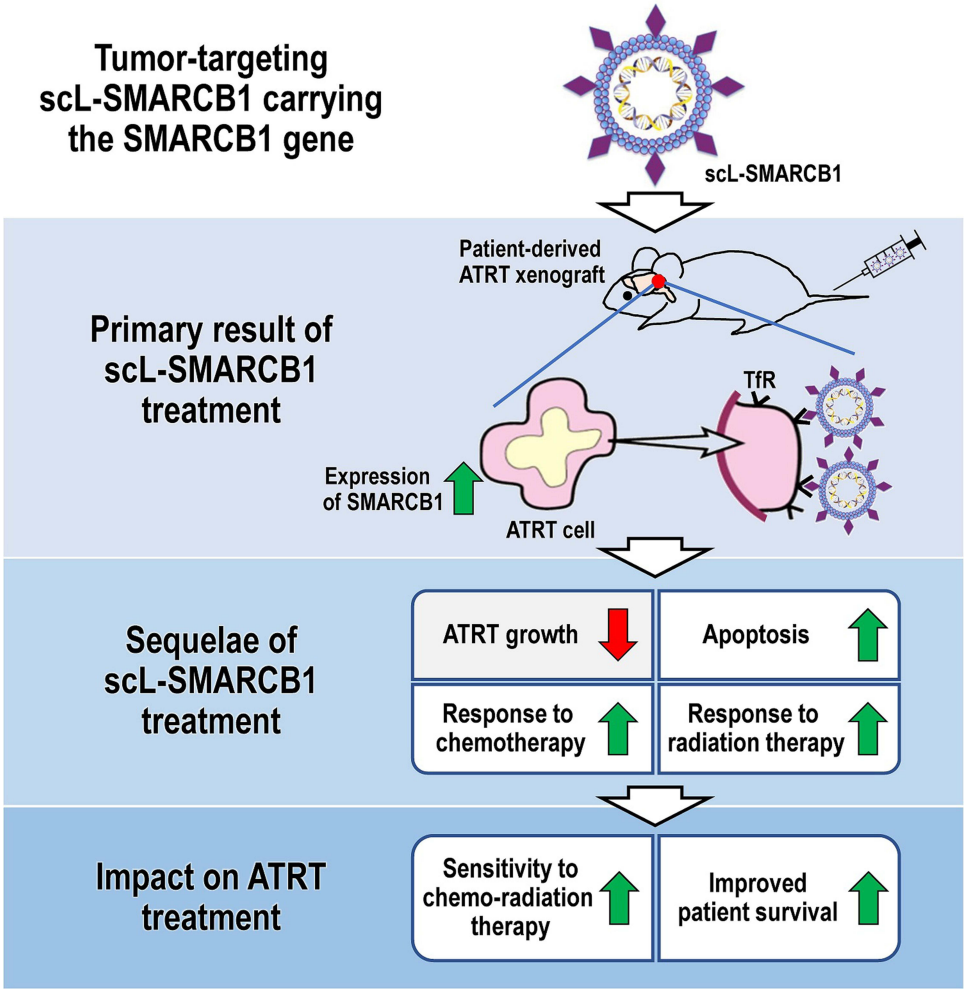

Although genomic instability is a common feature of most malignant cells,[5] ATRT genomes are highly stable. Most ATRTs contain less than ten coding mutations, and large chromosome gain or loss is uncommon.[6–8] The only recurring molecular abnormality that characterizes ATRT is the inactivation of the SMARCB1 gene, which is observed in nearly 98% of ATRT patients.[9] SMARCB1 encodes a core subunit of the SWI/SNF chromatin remodeling complex that contributes to developmental processes. Although up to 20% of human cancers contain a loss-of-function mutation in the SWI/SNF complex, its role in tumor suppression remains understudied.[10] It was only recent that several studies have revealed that SMARCB1 is a tumor suppressor with its loss required for rhabdoid tumorigenesis.[3,11] The precise mechanism through which SMARCB1 can act as a tumor suppressor remains to be fully understood.[7,11–15] In rhabdoid tumors, inactivation of SMARCB1 can drive proliferation by altering the expression of multiple pro-oncogenic pathways.[16–22] Importantly, loss of SMARCB1 also reduces the efficacy of conventional anti-cancer treatments, such as radiation and chemotherapy.[23,24] Thus, restoration of SMARCB1 is an attractive approach for treating patients with ATRT with the potential to render their ATRT more sensitive to conventional therapeutic modalities.

Combining emerging knowledge regarding SMARCB1 with nanotechnology, which enables brain tumor-targeted gene delivery, we assessed the potential of SMARCB1 restoration in ATRT using our nanomedicine (termed scL-SMARCB1). scL-SMARCB1 is an immuno-liposome nanocomplex decorated with anti-transferrin receptor single-chain antibody fragments (TfRscFv) that serves as a targeting moiety. Many types of cancer cells overexpress TfR to meet the increased demand for iron

to support their rapid growth.[25] Thus, TfRscFv allows our nanocomplex to efficiently deliver its cargo (ie, SMARCB1 transgene) into tumor cells. Moreover, our nanocomplex can actively enter and deliver payloads to intracranial tumors by traversing the blood-brain barrier (BBB) via TfR-mediated transcytosis.[26–28] Here, we performed translational studies using patient-derived ATRT cells and xenograft tumors to demonstrate the potential of scL-SMARCB1 as a novel therapy for this rare and fatal childhood cancer. We also studied the potential synergism between scL-SMARCB1 treatment and traditional anticancer treatment modalities, ie, radiation and chemotherapy.

Materials and Methods

Cell Lines

The human ATRT cell line BT-12 was obtained from Children's Oncology Group (Monrovia, CA, USA). Human ATRT cell line CHLA-06 and human rhabdomyosarcoma cell lines A-204 and Hs729 were obtained from the American Type Culture Collection (Manassas, VA, USA). The cells were maintained at 37°C in an atmosphere of 5% CO_2 in RPMI-1640 (Cytiva, Marlborough, MA, USA) supplemented with 15% FBS (Sigma, St. Louis, MO, USA; for BT-12), McCoy's 5A (Corning Cellgro, Corning, NY, USA) supplemented with 10% FBS (for A-204), DMEM (Corning Cellgro) supplemented with 10% FBS (for Hs729), or DMEM/F-12 (Corning Cellgro) supplemented with 20 ng/mL human FGF (Thermo Fisher, Waltham, MA), 20 ng/mL human EGF (Thermo Fisher), and 1× B27 supplement (Thermo Fisher; for CHLA-06). All experiments were performed using mycoplasma-free cells.

Plasmids

Sequence-verified human SMARCB1 full-length cDNA clone was obtained from the Mammalian Gene Collection at Horizon (Clone ID: 40125665). The SMARCB1 expression plasmid, pSCMV-SMARCB1 contains a 1.4-kb human wild-type (wt) SMARCB1 cDNA under the control of the cytomegalovirus (CMV) promoter, followed by the simian virus 40 (SV40) polyadenylation signal. The control plasmid, pSCMV, was an empty vector without the SMARCB1 insert.[29] All the plasmids were expanded in *E. coli* and purified using EndoFree Plasmid Mega/Giga kits (Qiagen, Germantown, MD, USA). Purified plasmids were quantified spectrophotometrically at A260/A280 >1.95.

Nanocomplex Preparation

Cationic liposome consisting of 1,2-dioleoyl-3-trimethylammonium propane (DOTAP, Avanti Polar Lipids, Alabaster, AL) and dioleolylphosphatidyl ethanolamine (DOPE; Avanti Polar Lipids), referred to as Lip, was prepared as described previously.[25] Briefly, DOTAP:DOPE (1:1 molar ratio) in ethanol were injected quickly into 55°C water in a test tube while vortexing. The solution was vortexed for an additional 20 min while cooling down to room temperature. Plasmid DNA carrying the human SMARCB1 gene (pSCMV-SMARCB1) or a control plasmid without the SMARCB1 insert (pSCMV) was encapsulated in TfRscFv/Lip (termed scL) immunoliposome nanocomplexes (scL-SMARCB1 or scL-vec, respectively), similar to a previously described method.[25] Briefly, the TfRscFv solution was mixed with Lip by gentle inversion for 10 min at room temperature to produce scL. Plasmid DNA was diluted in water and added to the scL at a DNA:lipid ratio of 1:8–1:14 (w/w ratio). The solution was mixed well for 10 min by inversion several times to produce the scL-SMARCB1 nanocomplex. The size and surface charge of the complexes were measured using a Zetasizer (Malvern Panalytical, Malvern, UK). For the cell culture experiments, the complex was further diluted with serum-free medium and added to the culture. For animal injections, 5% dextrose was added to the nanocomplex preparation.

Measurement of SMARCB1 Expression in vitro

To determine SMARCB1 expression, BT-12, CHAL-06, or A-204 cells were plated at 3.0×10^6 cells/10 cm dish for 24h before transfection. The scL-SMARCB1 nanocomplexes prepared as described above were diluted in serum-free medium and added to dishes (7μg DNA/dish). After incubation for 5h at 37°C, the medium was replaced with 10mL of fresh complete medium and the cells were further incubated. Cells were collected between 24 to 120h after transfection and subjected to either quantitative reverse transcription PCR (RT-qPCR) or western analysis. For Western blot analysis, the collected cells were lysed in cold radioimmunoprecipitation assay (RIPA) buffer containing protease inhibitors and 10μg

of total cellular protein was separated on 4–12% Bis-Tris Midi gels (Thermo Fisher, Waltham, MA), transferred to a nitrocellulose membrane, and hybridized with antibodies against human SMARCB1 (#91735, 1:1000 dilution, Cell Signaling, Danvers, MA, USA), followed by incubation in a horseradish peroxidase-conjugated anti-rabbit IgG (#7074S, 1:10,000 dilution, Cell Signaling). Antibodies recognizing human GAPDH (#2275-PC-100, 1:1000 dilution, Trevigen, Gaithersburg, MD, USA) were used as internal controls for protein loading. Chemiluminescent detection was performed using the SuperSignal West Dura Extended Duration Substrate (Thermo Fisher). Quantification of the protein bands was performed using the ImageJ software. For RT-qPCR, total RNA was extracted from the cell pellets using the PureLink RNA mini kit (Thermo Fisher) and reverse-transcribed using an iScript cDNA synthesis kit (Bio-Rad, Hercules, CA, USA). PCR was performed in triplicate using the TaqMan Fast Advanced Master Mix (Thermo Fisher) and TaqMan gene expression assays (Thermo Fisher) for human SMARCB1 (Hs00992521_m1) and GAPDH (Hs02786624_g1). RT-qPCR assays for transcript quantification were performed using the StepOnePlus RT-PCR system (Life Technologies), and relative mRNA expression levels were analyzed using StepOne software v2.3. via the ΔΔCt method, with normalization of the corresponding sample value for GAPDH.

Flow Cytometry

To determine TfR expression levels, BT-12, CHLA-06, and A-204 cells were stained with human CD71-FITC (anti-TfR; BioLegend, San Diego, CA) for 30 minutes at 4°C in the dark. After washing, the labeled cells were analyzed using a BD FACSAria flow cytometer (BD Biosciences, San Jose, CA, USA). To assess the level of apoptosis, cells were stained using the Annexin V/Dead Cell Apoptosis kit with propidium iodide (PI, Thermo Fisher) according to the manufacturer's protocol. The level of apoptosis was also assessed using cell cycle and sub-G1 analyses. After treatment, cells were harvested, washed with cold PBS, and fixed with ice-cold 75% ethanol. The fixed cells were washed twice with PBS and stained with 25μg/mL of PI. Cells were analyzed using an LSRFortessa flow cytometer (BD Biosciences). Cisplatin sensitization was assessed based on the level of apoptosis in BT-12 cells, as determined by the percentage of cells positive for Annexin V and PI staining. BT-12 cells (3.0×10^6 cells/10 cm dish) were treated with either scL-SMARCB1 or scL-vec nanocomplexes (7μg DNA/dish) for 24h, after which the cells were treated with 0.5μM of cisplatin. Seventy-two hours after the addition of cisplatin, the cells were collected, and the amount of apoptosis was assessed by flow cytometry, as described above.

Cell Viability Assay

Human ATRT (BT-12 and CHLA-06) and rhabdomyosarcoma (A-204 and Hs729) were plated at 3.0×10^3 cells/well in 96-well plates and 24h later treated with either scL-SMARCB1, scL-vec, or scL nanocomplex without payload at various concentrations in triplicates (0–250ng DNA/well). Forty-eight hours after treatment, cell viability was determined using the sodium 30-[1-(phenylamino-carbonyl)-3, 4-tetrazolium]-bis(4-methoxy-6-nitro)-benzenesulfonate (XTT) assay (Polysciences, Warrington, PA, USA). The IC_{50} values, the drug concentration resulting in 50% cell death, were interpolated from the graph of DNA concentration versus the fraction of surviving cells using SigmaPlot 11.2 (Systat Software, San Jose, CA, USA). To assess the degree of sensitization to cisplatin, BT-12, CHLA-06, and A-204 cells were treated with scL-SMARCB1 or scL-vec nanocomplexes (10–50ng DNA/well) for 24h, followed by the addition of increasing concentrations of cisplatin (0–100μM). Seventy-two hours after the addition of cisplatin, cell viability was determined using the XTT assay as described above. CHLA-06 cells were subjected to Western blot analysis using antibodies against SMARCB1 (#91735, 1:1000 dilution, Cell Signaling Technology), cleaved caspase-3 (cCasp3, #9661, 1:1000 dilution, Cell Signaling Technology), and cleaved poly (ADP-ribose) polymerase (cPARP, #9541, 1:1000 dilution, Cell Signaling Technology). Antibodies against GAPDH (#2275-PC-100, 1:1000 dilution, Trevigen) were used as internal controls for protein loading.

Senescence-Associated β-Galactosidase Staining and Western Blot Analysis

BT-12 and A-204 cells were plated in six-well plates at a density of 1.0×10^5 cells per well and transfected with either scL-vec or scL-SMARCB1 nanocomplexes as described above. Seven days after treatment, the cells were fixed and stained using a Senescence β-Galactosidase Staining Kit (Cell Signaling Technology), according to the manufacturer's protocol. Cells were photographed using an Olympus IX-71 inverted microscope (Olympus Life

Sciences, Waltham, MA, USA). The cells were also subjected to Western blot analysis using antibodies against CDKN2A (#80772, 1:1000 dilution, Cell Signaling Technology) and CDKN1A (#2947, 1:1000 dilution, Cell Signaling Technology). Antibodies recognizing Lamin B1 (#sc-377000, 1:1000 dilution, Santa Cruz Biotechnology, Dallas, TX, USA) were used as internal controls for protein loading.

In vivo Studies

All in vivo animal experiments were approved by the Georgetown University Institutional Animal Care and Use Committee (IACUC). All experiments were performed in accordance with the approved GUACUC protocols of the Georgetown University. For the subcutaneous tumor model, 6-week-old female athymic nude mice (Hsd:Athymic Nude-Foxn1nu, Envigo, Indianapolis, IN) were inoculated on their flanks with BT-12 cells (2.0×10^6 cells/site). For the intracranial tumor model, 6-week-old female athymic nude mice were stereotactically inoculated in the right hemisphere of the mouse brain (2.0 mm posterior to lambda, 1.5 mm lateral to midline, and 3.0 mm depth from skull) with BT-12 cells (0.25×10^6 cells/mouse). Mice with established tumors were injected twice a week for 6 injections of scL-SMARCB1 (30μg DNA/injection, intravenously administered). In some experiments, 2 mg/kg cisplatin was administered once a week for a total of three injections via intraperitoneal injection 24h after injection of scL-SMARCB1 injection. In some experiments, 24h after the initial injection of scL-SMARCB1, the animals were secured in a lead restraint that permitted only the tumor area to be exposed to γ-irradiation, and the first fractionated dose of 5 Gy of ionizing radiation was administered. Thereafter, the animals were administered with 5 Gy on the indicated days to a total dose of 15 Gy per mouse. We monitored the body weight of the tumor-bearing mice and evaluated the in vivo response based on changes in tumor volume over time. The size of the subcutaneous tumor was measured semi-weekly and the tumor volume (L×W×H) was in mm^3 calculated. The size of the intracranial tumor was measured by magnetic resonance imaging (MRI). Transcriptional changes in genes related to cancer progression were tested by RT-qPCR in intracranial BT-12 tumors harvested at 72h after a single injection of scL-SMARCB1 nanocomplex (30μg DNA). Total RNA was extracted from the brain tumors using a RNeasy Plus Mini Kit (QIAGEN) and reverse transcribed using an iScript cDNA synthesis kit (Bio-Rad). PCR was performed in triplicate using TaqMan Fast Advanced Master Mix (Thermo Fisher) and TaqMan gene expression assays (Thermo Fisher) for human SMARCB1 (Hs00992521_m1), CDKN1C (Hs00908986_g1), CDKN2A (Hs00923894_m1), GADD45A (Hs00169255_m1), MYC (Hs00153408_m1), HSPE1 (Hs01654720_g1), CDK4 (Hs00260861_m1), AURKA (Hs01582072_m1), and GAPDH (Hs02786624_g1), as described above.

Magnetic Resonance Imaging

To visualize and measure intracranial tumors, animals were imaged in vivo without the aid of a contrast agent on a 7T Bruker horizontal spectrometer/imager run using Paravision 5.1 software (Bruker Biospin MRI GmbH, Karlsruhe, Germany). ImageJ software was used to calculate tumor volumes. The regions of interest (ROIs) containing tumors were determined based on the contrast differential exhibited by brain tumors versus normal brains and manually traced. The volumes were determined by multiplying the area by slice thickness.

Blood Analysis

To assess the potential non-specific toxicity associated with the treatments, blood was collected for serum chemistry analysis (Antech Diagnostics) from BT-12 bearing mice treated with either cisplatin in combination with radiation or scL-SMARCB1 in combination with radiation on days 35 and 56 (n=5 per group).

Statistical Analysis

Data are presented as the mean ± standard deviation. Statistical significance was determined using a one-way ANOVA or Student's *t*-test. Statistical significance was set at $P < 0.05$. The Log rank test was used for the survival studies. All graphs and statistical analyses were performed using the SigmaPlot 11.2.

Results

Characterization of scL-SMARCB1 Nanocomplex

The size (Figure 1A) and zeta potential (Figure 1B) of the freshly prepared nanocomplexes were measured using dynamic light scattering (DLS) method. The empty nanocomplex without the payload (termed scL) measured approximately 29.27 ± 2.02 nm in size (diameter) with a zeta potential of 56.89 ± 1.24 mV (Figure 1C). When the DNA payload was encapsulated in the nanocomplex, the particle size increased, whereas the surface charge decreased. The average size of scL-SMARCB1 nanocomplex was 113.38 ± 13.38 nm with a zeta potential of 27.90 ± 0.37 mV. The size of a control nanocomplex that carries plasmid DNA without SMARCB1 insert (termed scL-vec) was 113.93 ± 17.86 nm with a zeta potential of 30.05 ± 0.28 mV. The nanocomplexes encapsulating DNA plasmid payloads (ie, scL-SMARCB1 and scL-vec) were similar in size and surface charge. These complexes were in the nanosize range, and their small polydispersity index (PDI) values indicated a homogenous population of nanocomplexes (Figure 1C). In our previous effort to characterize scL nanocomplex encapsulating TP53 plasmid DNA (scL-p53) by cryogenic electron microscopy and atomic force microscopy, a virus-like structure of nanocomplex with ~100 nm in diameter was observed.[26] Agarose gel motility shift assay of the same nanocomplex demonstrated that when prepared using the optimal ratio, >99.5% of the plasmid DNA used in the preparation of the nanocomplex was encapsulated.[26] scL-SMARCB1 differs from scL-p53 nanocomplex only in the identity of the tumor suppressor cDNA present in the plasmid DNA component; the targeting single-chain monoclonal antibody and the cationic liposome are identical. Thus, similar morphology and encapsulation efficiency are expected with scL-SMARCB1. When siRNA was encapsulated in scL

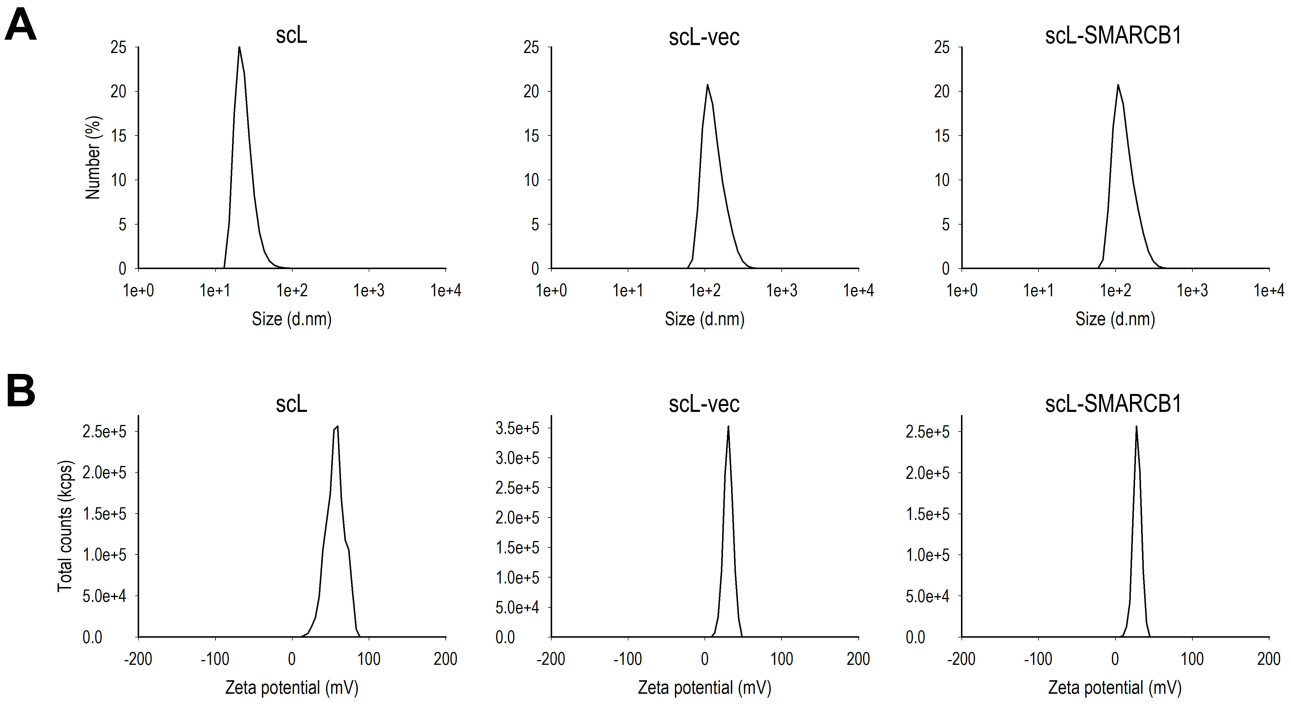

C

Nanocomplex	PDI	Number (d.nm)	Volume (d.nm)	Intensity (d.nm)	Zeta Potential (mV)
scL	0.27 ± 0.01	29.27 ± 2.02	50.19 ± 7.17	113.20 ± 14.42	56.89 ± 1.24
scL-vec	0.16 ± 0.04	113.93 ± 17.86	186.97 ± 3.30	196.40 ± 2.95	30.05 ± 0.28
scL-SMARCB1	0.15 ± 0.03	113.38 ± 13.38	180.05 ± 6.54	188.77 ± 7.42	27.90 ± 0.37

Figure 1 Characterization of scL-SMARCB1 nanocomplex. (**A**) Size distribution of scL-SMARCB1 nanocomplex, control nanocomplex containing a plasmid without the SMARCB1 insert (scL-vec), and empty nanocomplex, ie, lacking a DNA payload (scL). Shown are the data from analyses using a Malvern Zetasizer expressed as the number average values. (**B**) Zeta potential (surface charge) of nanocomplexes. (**C**) A compilation of the polydispersity index (PDI), size distribution (by number, volume, and intensity), and zeta potential values of nanocomplexes is shown (N = 3–5/nanocomplex).

nanocomplex, the serum stability of siRNA was significantly improved that intact scL-siRNA is clearly present in circulation for at least 24h after an intravenous administration in mice, while free siRNA without delivery system was undetectable at 3h in blood (unpublished data), suggesting a similar stability of scL-SMARCB1 nanocomplex in vivo.

scL-SMARCB1 Treatment Restores SMARCB1 Expression in SMARCB1-Deficient Rhabdoid Tumor Cells

Compared to normal cells, tumor cells maintain many times higher level of TfR expression on their surface in response to increased iron demand.[30] It was also shown that TfR level can be correlated with tumor stage or cancer progression.[31] In our study, TfR serves as the binding target for receptor-mediated endocytosis into rhabdoid tumor cells via the TfRscFv targeting moiety that decorates the surface of scL-SMARCB1 nanocomplex. In a number of our earlier studies, we have demonstrated the importance of the targeting moiety for the increased transfection efficiency and tumor targeting ability of the scL nanocomplex when compared to both a control antibody and unliganded complex without targeting moiety in vitro and in vivo.[32] Thus, we first validated the expression of TfRs on the surface of rhabdoid tumor cells to assess the feasibility of delivering payloads into these cells via TfR-mediated endocytosis. Flow cytometric analysis demonstrated the positive expression of TfR in patient-derived ATRTs (BT-12 and CHLA-06) and rhabdomyosarcoma (A-204), indicating the potential of scL-SMARCB1 nanocomplex to deliver therapeutics to these tumor cells (Figure 2A). Previously, we have examined the intracellular uptake and subcellular localization of scL nanocomplex that carries fluorescently labeled (6FAM-) oligonucleotides as a model payload to allow tracking of nanocomplexes intracellularly.[33] A time lapse imaging using total internal reflection fluorescence (TIRF) microscopy of in vitro transfection of human colorectal cancer HT-29 cells leveled a significant accumulation of payload (6FAM-ODN) in the cytoplasm as early as 3h after transfection, and the signal intensified over time as more nanocomplex were taken up by the cells and intracellularly accumulating. Although we did not evaluate the uptake of scL-SMARCB1 nanocomplex, a similar uptake of nanocomplex can be anticipated. We further investigated whether the scL-SMARCB1 nanocomplex could successfully restore the exogenous SMARCB1 expression in these cells. The SMARCB1-deficient ATRT cell line BT-12 was transfected with scL-SMARCB1 or scL-vec nanocomplexes. The transcriptional expression of SMARCB1 was monitored by RT-qPCR at 24, 48 and 72h after transfection (Figure 2B, left panel). Significantly higher levels of SMARCB1 mRNA were detected in BT-12 cells treated with the scL-SMARCB1 nanocomplex across all time points, but not in BT-12 cells treated with scL-vec, than in untreated cells. Furthermore, Western blot analysis of BT-12 cells treated with scL-SMARCB1 showed distinct bands of the exogenous SMARCB1 protein at 44kDa at all time points (Figure 2C). However, cells that were untreated or treated with scL-vec showed no detectable expression of the SMARCB1 protein at any time point. It has been reported that main subcellular locations of SMARCB1 protein are nucleus and cytosol.[34] Although we did not study the subcellular distribution of the restored SMARCB1 protein, using scL nanocomplex carrying GFP plasmid DNA as a model payload (scL-GFP), we have previously examined subcellular localization of exogenous GFP protein in human colorectal cancer (HT-29) and human glioblastoma (U251 and U87) cell lines.[33] We have observed a strong nuclear expression and lower cytoplasmic expression of exogenous GFP in all three cancer cell lines. We anticipate a similar distribution of exogenous SMARCB1 protein in the nucleus and cytosol. We also validated the restoration of SMARCB1 expression in two other SMARCB1-deficient rhabdoid tumor cell lines, CHLA-06 and A-204. Both cell lines were transfected with either scL-SMARCB1 or scL-vec nanocomplexes and tested for SMARCB1 mRNA levels 48 and 120h later using RT-qPCR. Similar to BT-12, a significant increase in SMARCB1 mRNA levels was observed in both CHLA-06 and A-204 cells transfected with the scL-SMARCB1 nanocomplex (Figure 2B, middle and right panels, respectively) compared with untreated cells, whereas the scL-vec nanocomplex did not change SMARCB1 expression. Collectively, these results confirmed the ability of the scL-SMARCB1 nanocomplex to deliver SMARCB1 gene and restore SMARCB1 expression in multiple rhabdoid tumor cell lines that are otherwise deficient in SMARCB1.

scL-SMARCB1 Inhibits Growth of SMARCB1-Deficient Rhabdoid Tumor Cells

We have assessed the antitumor effects of SMRACB1 restoration on various rhabdoid tumor cells. SMARCB1-deficient ATRTs (BT-12 and CHLA-06), SMARCB1-deficient rhabdomyosarcoma (A-204), and SMARCB1-expressing rhabdomyosarcoma (Hs729) cells were treated with scL-SMARCB1 or scL-vec nanocomplexes at various concentrations (0−250ng DNA/well).

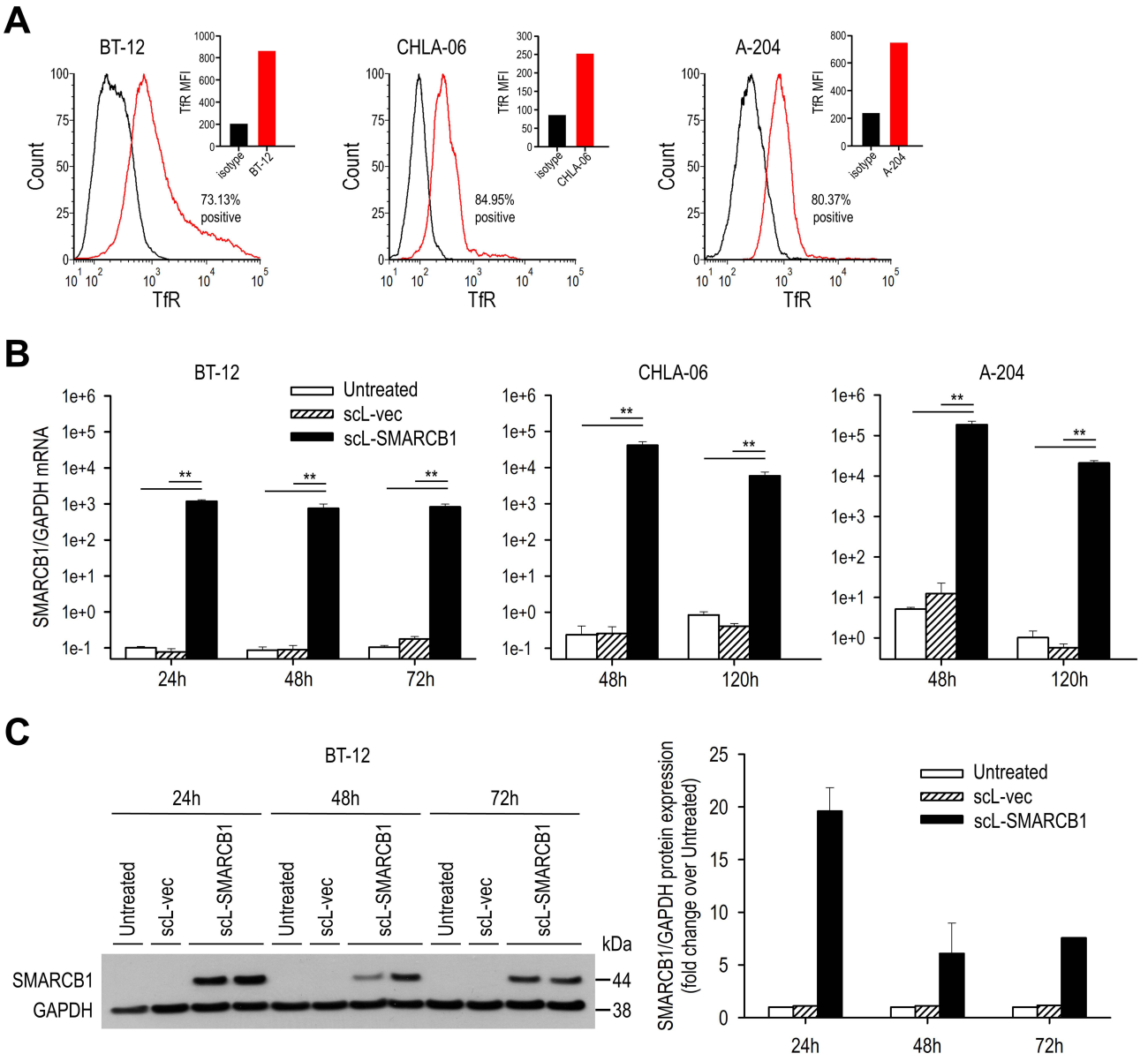

Figure 2 scL-SMARCB1 nanocomplex restores SMARCB1 expression in SMARCB1-deficient rhabdoid tumor cells. (**A**) Flow cytometric analysis of TfR expression on the surface of patient-derived ATRT (BT-12 and CHLA-06) and rhabdomyosarcoma (A-204). Median fluorescence intensity (MFI) is shown in top-right corners. (**B**) RT-qPCR analysis of transcriptional expression of SMARCB1 at indicated time after transfection with either scL-SMARCB1 or scL-vec (N = 4 for BT-12, N = 3 for CHLA-06 and A-204). **p<0.01. (**C**) Western blot analysis of SMARCB1 expression in BT-12 cells treated with either scL-SMARCB1 or scL-vec (left panel). A densitometric analysis of Western blot results presented (right panel).

Forty-eight hours later, tumor cell survival was determined using the XTT assay. In all SMARCB1-deficient cells, transfection with scL-SMARCB1 nanocomplex resulted in a dose-dependent killing of tumor cells with IC_{50} of 137.32ng, 128.60ng, and 19.92ng of DNA/well in BT-12, CHLA-06, and A-204 cells, respectively (Figure 3A). However, neither scL nor scL-vec demonstrated a similar antitumor effect with an equivalent amount of nanocomplex, indicating that antitumor activity is due to the restoration of exogenous SMARCB1 rather than the delivery system itself. Importantly, treatment of SMARCB1-expressing Hs729 cells with the scL-SMARCB1 nanocomplex did not induce antitumor activity with an IC_{50} value of >250ng of DNA/well, suggesting that SMARCB1 re-expression does not produce antitumor effects in SMARCB1-expressing cells. We further investigated whether the observed antitumor activity was associated with activation of cellular apoptosis. Flow cytometric analysis of A-204 cells at 72h after the transfection with scL-SMARCB1 nanocomplex showed a significant increase in the early (Annexin V^+PI^-) and late (Annexin V^+PI^+) apoptotic populations compared with the untreated control (Figure 3B). However,

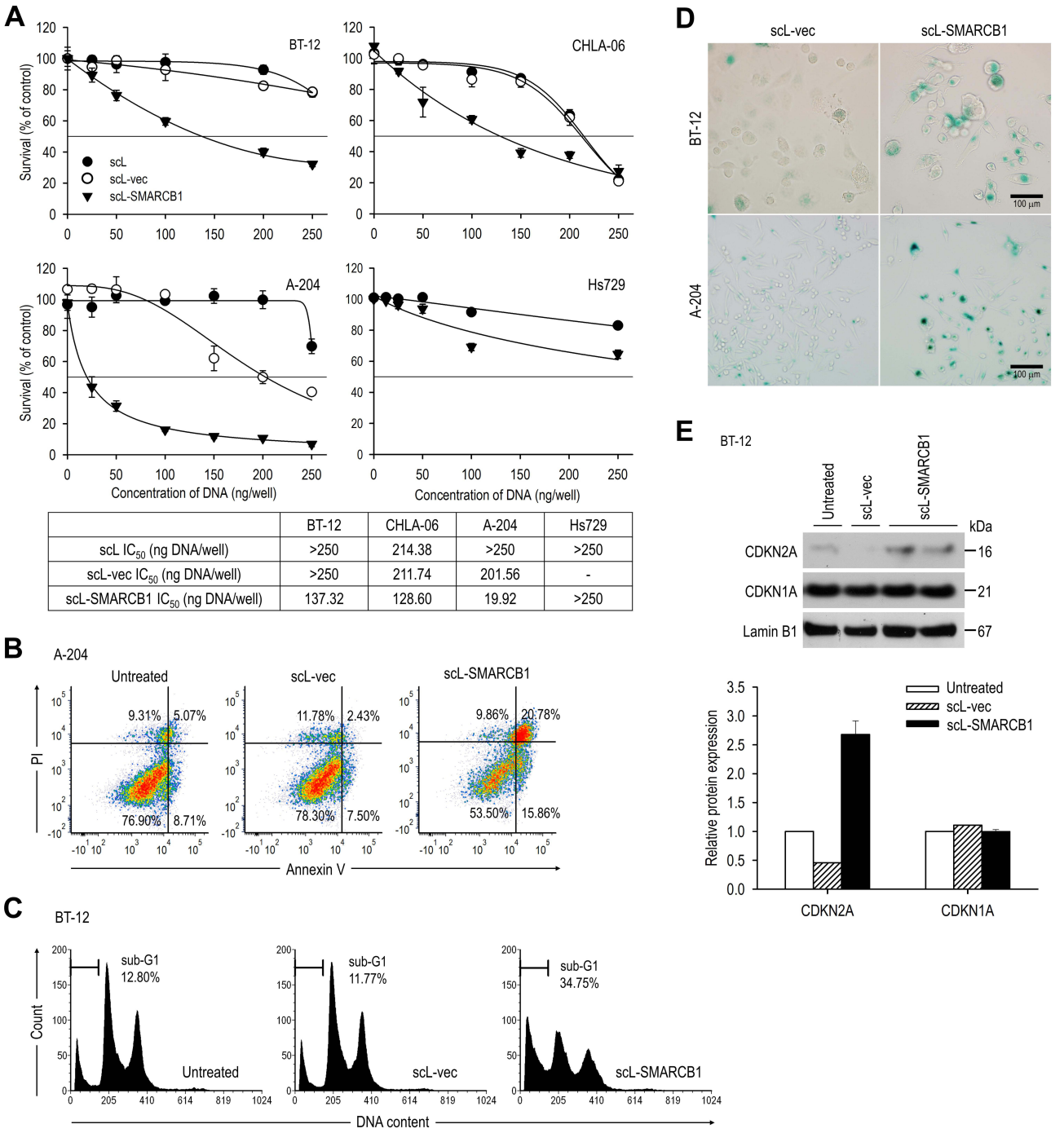

	BT-12	CHLA-06	A-204	Hs729
scL IC_{50} (ng DNA/well)	>250	214.38	>250	>250
scL-vec IC_{50} (ng DNA/well)	>250	211.74	201.56	-
scL-SMARCB1 IC_{50} (ng DNA/well)	137.32	128.60	19.92	>250

Figure 3 scL-SMARCB1 nanocomplex inhibits growth of SMARCB1-deficient rhabdoid tumor cells. SMARCB1-deficient ATRT (BT-12 and CHLA-06), SMARCB1-deficient rhabdomyosarcoma (A-204), and SMARCB1-expressing rhabdomyosarcoma (Hs729) were transfection with increasing concentrations of either scL-SMARCB1, scL-vec, or an empty nanocomplex without payload (scL). (**A**) XTT cell viability assay at 48h after transfection. A compilation of the IC_{50} values is shown (lower panel). (**B**) Induction of apoptosis was monitored via Annexin V/PI staining in A-204. Numbers in the quadrants indicate the percentage of cells in each quadrant. (**C**) Cell cycle analysis of BT-12. Sub-G1 peaks represent apoptotic cells. (**D**) Representative photographs of senescence-associated β-galactosidase staining of BT-12 and A-204. The scale bars indicate 100 μm. (**E**) Western blot analysis of senescence associated cell cycle inhibitors (CDKN1A and CDKN2A) in BT-12 cells (top panel). A densitometric analysis of Western blot results presented (lower panel).

A-204 cells treated with scL-vec showed an insignificant increase in the Annexin V^+ fraction compared with the untreated control. In another experiment, flow cytometric analysis of the sub-G1 fraction, which is another characteristic of apoptosis, in BT-12 cells receiving scL-SMARCB1 treatment showed a significant increase in the apoptotic population compared to that in the untreated control at 72h post-treatment (Figure 3C). However, scL-vec treatment of BT-12 cells did not increase the sub-G1

fraction compared to the untreated control, validating that the antitumor activity was due to the restoration of exogenous SMARCB1. We also asked whether the anti-tumor activity of SMARCB1 restoration was associated with activation of senescence given that the reintroduction of SMARCB1 could cause senescence in rhabdoid tumors.[35] We first measured induction of senescence-associated β-galactosidase (SA-β-gal), a widely used biomarker for senescent cells. scL-SMARCB1 treatment, but not scL-vec treatment, strongly induced SA-β-gal activity (Figure 3D), demonstrating elevated senescence in BT-12 and A-204 cells seven days after treatment with the scL-SMARCB1 nanocomplex. Western blot analysis showed increased expression of senescence-associated CDKN2A in BT-12 cells treated with scL-SMARCB1 compared to that in untreated BT-12 cells (Figure 3E), indicating that SMARCB1-induced senescence via CDKN2A activation is another mechanism of inhibition of rhabdoid tumor progression. Collectively, our results indicate that re-expression of SMARCB1 in SMARCB1-deficient rhabdoid tumor cells results in reduced growth of cells expressing exogenous SMARCB1, undergoing apoptosis and senescence.

scL-SMARCB1 Inhibits BT-12 Tumor Growth in vivo

To determine the therapeutic potential of scL-SMARCB1 in ATRT, we assessed the response of ATRT xenografts to scL-SMARCB1 treatment. Athymic mice bearing subcutaneously established BT-12 tumors were treated with scL-SMARCB1 nanocomplex via tail vein injections (30μg DNA/injection), as shown in Figure 4A, and tumor growth was monitored. During the treatment period (between days 8 and 26), there was significant inhibition of tumor growth in animals receiving scL-SMARCB1 (1.6-fold increase from their initial tumor volume) compared to animals without any treatment (3.5-fold increase from their initial size) (Figure 4B). The inhibition of tumor growth continued even after the treatment was stopped. At harvest on day 43 (ie, 17 days after the last treatment), tumors from untreated control mice weighed approximately twice as heavy as tumors from mice treated with scL-SMARCB1 (Figure 4C), demonstrating the significant anti-tumor effect of scL-SMARCB1 as a single-agent treatment. Importantly, the body weights of tumor-bearing animals did not differ significantly between the untreated control and scL-SMARCB1 treatment groups, indicating little, if any, systemic toxicity (Figure 4D). Taken together, these data indicated that the restoration of exogenous SMARCB1 via the scL-SMARCB1 nanocomplex effectively suppressed the growth of SMARCB1-deficient tumors.

scL-SMARCB1 Improves the Survival of Mice Bearing Intracranial BT-12 Tumor

To further determine in vivo efficacy of scL-SMARCB1, we performed a survival study using athymic mice bearing intracranially established BT-12 tumors. Twelve days after tumor inoculation, brain tumors were confirmed in the cerebellum of the mouse brain by MRI, and treatment was initiated on day 14 (Figure 5A). As was seen in the subcutaneous tumor model, significant growth inhibition of BT-12 tumors was observed with scL-SMARCB1 treatment compared to the untreated control group (Figures 5B and C). However, scL-vec treatment did not affect tumor growth. On day 49, MRI-based measurement of tumor volume revealed a significantly smaller tumor size with scL-SMARCB1 treatment compared with the untreated control (6.1-fold versus 18.8-fold increase from their initial size on day 12, respectively). During the treatment period, the body weight of tumor-bearing mice in the untreated control group and the scL-vec-treated group decreased rapidly, indicating poor health of mice with a significant tumor burden (Figure 5D). In comparison, the body weight of mice receiving scL-SMARCB1 treatment remained stable for an extended period before rapidly decreasing as the tumor burden increased. Without any treatment, all mice succumbed to brain tumors before day 69, with a median survival of 51 days (Figure 5E). However, mice that received scL-SMARCB1 therapy survived for a significantly longer period (up to 99 days), with a median survival time of 74 days. In contrast, scL-vec treatment resulted in no demonstrable survival benefit. We next addressed whether the observed antitumor activity of scL-SMARCB1 was accompanied by transcriptional modulation of genes related to cancer progression. RT-qPCR analysis of intracranial BT-12 tumors harvested at 72h after a single injection of the scL-SMARCB1 nanocomplex (30μg DNA) showed a significant upregulation of SMARCB1 mRNA compared to untreated tumors, but this was not observed in tumors treated with scL-vec (Figure 5F). This result confirmed the ability of the scL-SMARCB1 nanocomplex to deliver SMARCB1 gene and restore SMARCB1 expression in intracranial tumors after systemic administration. Importantly, scL-SMARCB1 treatment, but not scL-vec treatment, significantly upregulated the expression of MYC-repressed genes (CDKN1C, CDKN2A, and GADD45A), while downregulating MYC-activated genes (HSPE1 and CDK4) compared to untreated tumors (Figure 5F). In addition, scL-SMARCB1 treatment significantly downregulated AURKA, which plays a critical role in mitosis and ATRT tumorigenesis.[36] Taken together, these data indicate that the systemically administered scL-

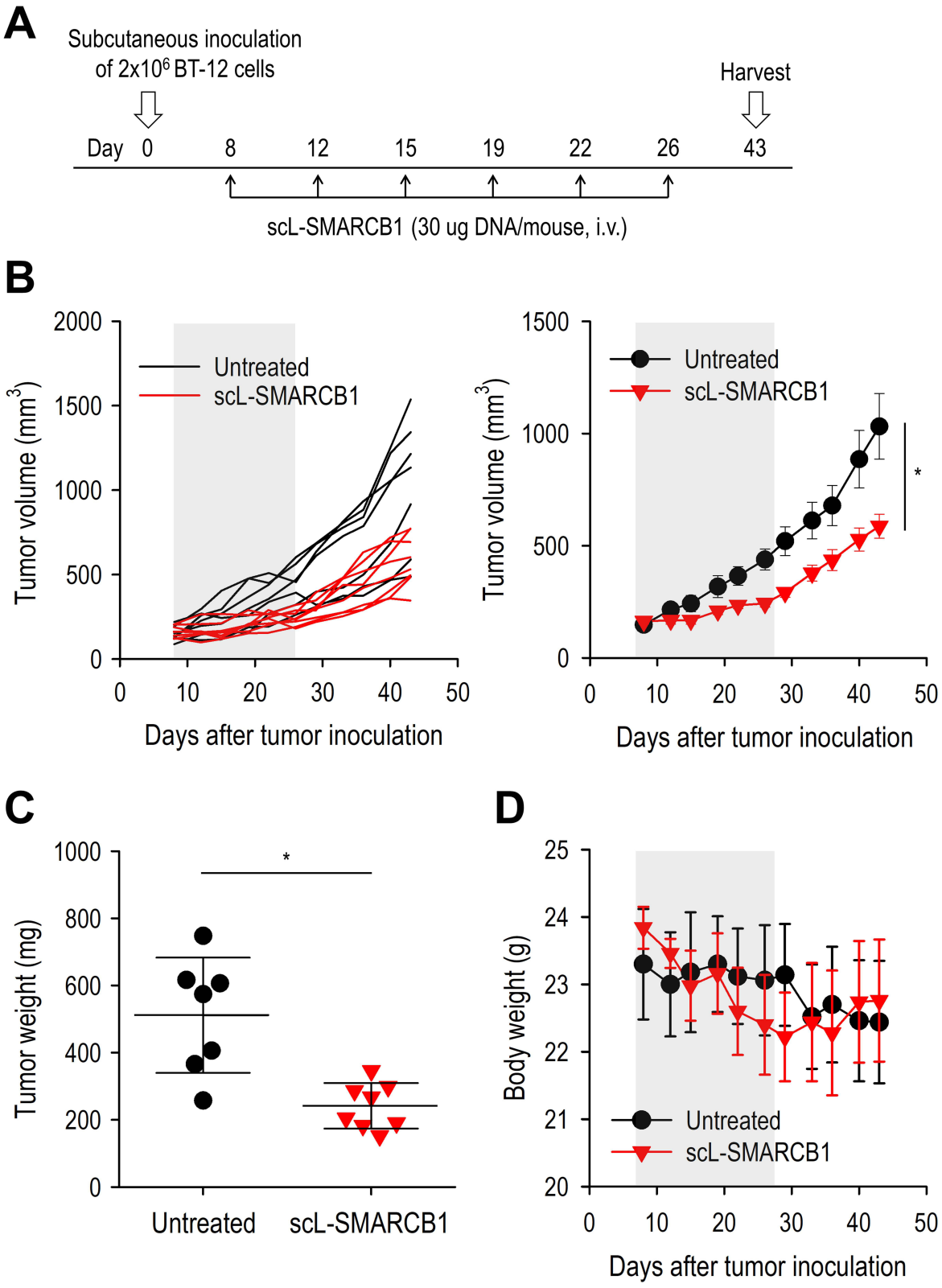

Figure 4 scL-SMARCB1 nanocomplex inhibits BT-12 tumor growth in vivo. Athymic mice with subcutaneous BT-12 tumor xenografts were randomized to therapy with scL-SMARCB1. (**A**) Treatment schedule. Mice received total 6 injections of scL-SMARCB1 (30 μg/injection, twice weekly for 3 weeks, N = 7 for untreated group, N = 8 for scL-SMARCB1 group). (**B**) Comparison of tumor growth between treatment groups. Tumor volumes are shown for individual tumor (left panel) and on average (right panel). Gray boxes indicate the treatment period. *p<0.05. (**C**) Quantification of tumor weight at harvest on day 43. *p<0.05. (**D**) Comparison of body weight changes between treatment groups.

https://doi.org/10.2147/IJN.S458323 DovePress

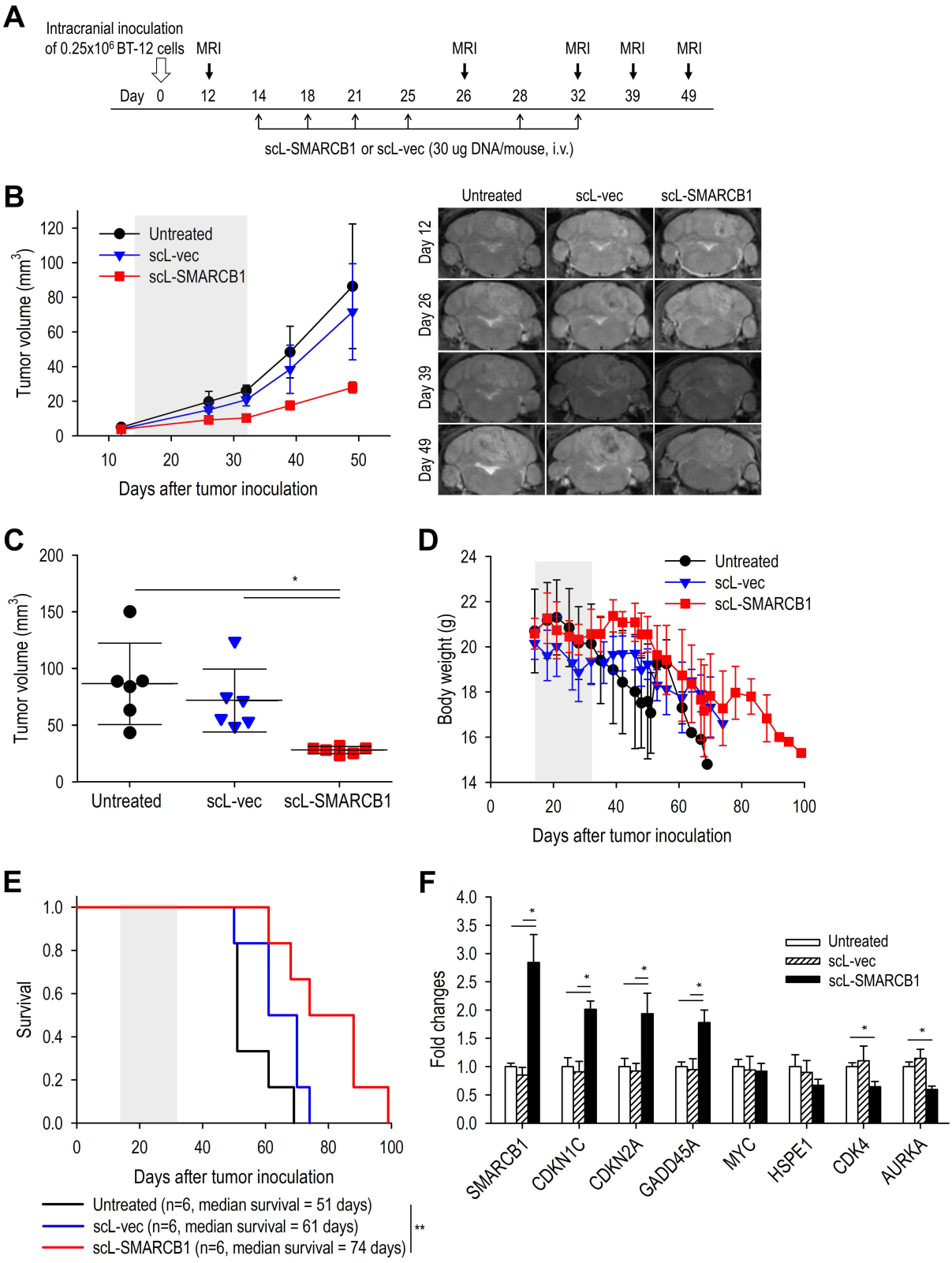

Figure 5 scL-SMARCB1 nanocomplex improves the survival of mice bearing intracranial BT-12 tumor. Athymic mice with intracranial BT-12 tumor xenografts were randomized to therapy with scL-SMARCB1 or scL-vec. (**A**) Treatment schedule. Mice received total 6 injections of scL-SMARCB1 (30 μg/injection, twice weekly for 3 weeks, N = 6/group). (**B**) Comparison of tumor growth between treatment groups (left panel). MRI images were evaluated to determine tumor volume. Representative MRI images (right panel). Gray box indicates the treatment period. *p<0.05. (**C**) MRI-based measurement of tumor volume on day 49. *p<0.05. (**D**) Comparison of body weight changes between treatment groups. (**E**) Kaplan–Meier survival curves of mice. Log Rank test, **p<0.01. N = 6/group. (**F**) RT-qPCR analysis of transcriptional expression of genes related to ATRT progression. *p<0.05.

SMARCB1 nanocomplex restored functional SMARCB1 expression in intracranial tumors and effectively suppressed the growth of SMARCB1-deficient tumors, leading to the extended survival of tumor-bearing mice. These observations support the contention that restoration of SMARCB1 via the scL-SMARCB1 nanocomplex could be an effective therapeutic strategy for treating patients with ATRT.

scL-SMARCB1 Promotes Cisplatin-Induced Cytotoxicity in ATRT

It has been suggested that the loss of SMARCB1 might limit the efficacy of traditional anti-cancer treatments, such as ionizing radiation and chemotherapeutic agents.[23,24] Thus, we further studied the effect of combining scL-SMARCB1 with conventional therapeutic modalities. Although multi-agent chemotherapy regimens vary greatly among patients, platinum-based chemotherapy is widely used as a mainstay in the treatment of ATRT patients.[37] Thus, we tested whether SMARCB1 restoration by scL-SMARCB1 would potentiate cisplatin therapy in ATRT. BT-12, CHLA-06, and A-204 cells were transfected with scL-SMARCB1 for 24h and treated with increasing concentrations of cisplatin for an additional 72h. Cells treated with either cisplatin alone or cisplatin in combination with scL-vec were used as the controls. The XTT assay revealed that the addition of scL-SMARCB1 to cisplatin significantly increased the effectiveness of killing malignant rhabdoid tumor cells relative to cisplatin monotherapy (Figure 6A). In contrast, there was a minimal or no increase in the effectiveness of killing tumor cells when scL-vec was added to cisplatin. These results demonstrate that the increased response to cisplatin was due to the presence of exogenous SMARCB1 protein and not non-specific cytotoxicity. In addition, flow cytometric analysis showed a significant increase in the early (Annexin V^+PI^-) and late (Annexin V^+PI^+) apoptotic populations in BT-12 cells receiving cisplatin in combination with scL-SMARCB1 treatment compared to cells receiving cisplatin only (Figure 6B). However, adding scL-vec to cisplatin treatment did not increase the Annexin V^+ fraction compared with cisplatin monotherapy. Apoptosis induction was further monitored by Western blotting for cleaved caspase-3 (cCasp3) and cleaved poly(ADP-ribose) polymerase (cPARP), common apoptosis markers, in CHLA-06 cells (Figure 6C). With the combination therapy of scL-SMARCB1 and cisplatin, the expression of both cCasp3 and cPARP was substantially increased compared to cisplatin monotherapy. However, there was no significant upregulation of apoptosis markers with the combination of scL-vec and cisplatin. Taken together, these results suggest that SMARCB1 restoration in combination with cisplatin can promote apoptosis in ATRT cells.

We continued to study the in vivo effects of SMARCB1 restoration in combination with cisplatin treatment in human ATRT. Athymic mice bearing intracranially established xenografts of BT-12 were treated with scL-SMARCB1 via tail vein injections (30μg DNA/injection), cisplatin via IP injections (2 mg/kg), or a combination of both (Figure 6D). The presence of tumors was confirmed in the mouse brain using MRI, and treatment was initiated 13 days after tumor inoculation. In line with in vitro study, significant inhibition of tumor growth was evident with the combination treatment of scL-SMARCB1 and cisplatin, as monitored by MRI (Figure 6E). While either cisplatin or scL-SMARCB1 as a single-agent therapy had a moderate inhibitory effect on tumor growth, tumors from mice that received the combination of scL-SMARCB1 and cisplatin demonstrated significantly stronger anti-tumor responses. However, the combination of cisplatin and scL-vec displayed an antitumor effect similar to that of the cisplatin monotherapy. Importantly, there was a significant difference in survival when scL-SMARCB1 was administered in combination with cisplatin compared with cisplatin alone (Figure 6F). Without any treatment, all mice succumbed to their disease before day 77, with a median survival of 56 days. However, addition of scL-SMARCB1 to cisplatin treatment significantly improved survival, with a median survival time of 80 days. In contrast, mice receiving either cisplatin plus scL-vec or cisplatin alone had a median survival of only 69 days. Collectively, the addition of scL-SMARCB1 to cisplatin treatment promoted cisplatin-induced cytotoxicity in vivo and significantly improved the survival of ATRT-bearing mice.

scL-SMARCB1 Promotes Radiation-Induced Cytotoxicity in ATRT

We have also studied whether scL-SMARCB1 could enhance radiation therapy, an established treatment for pediatric brain tumors associated with better survival.[3] Athymic mice bearing intracranially established xenografts of BT-12 were treated with either whole brain radiation (5 Gy), scL-SMARCB1 via tail vein injections (30μg DNA/injection), or combination of both as shown in Figure 7A. We also tested cisplatin treatment in combination with radiation therapy, because chemoradiation therapy is routinely used for the treatment of pediatric brain tumors. After confirming the tumor

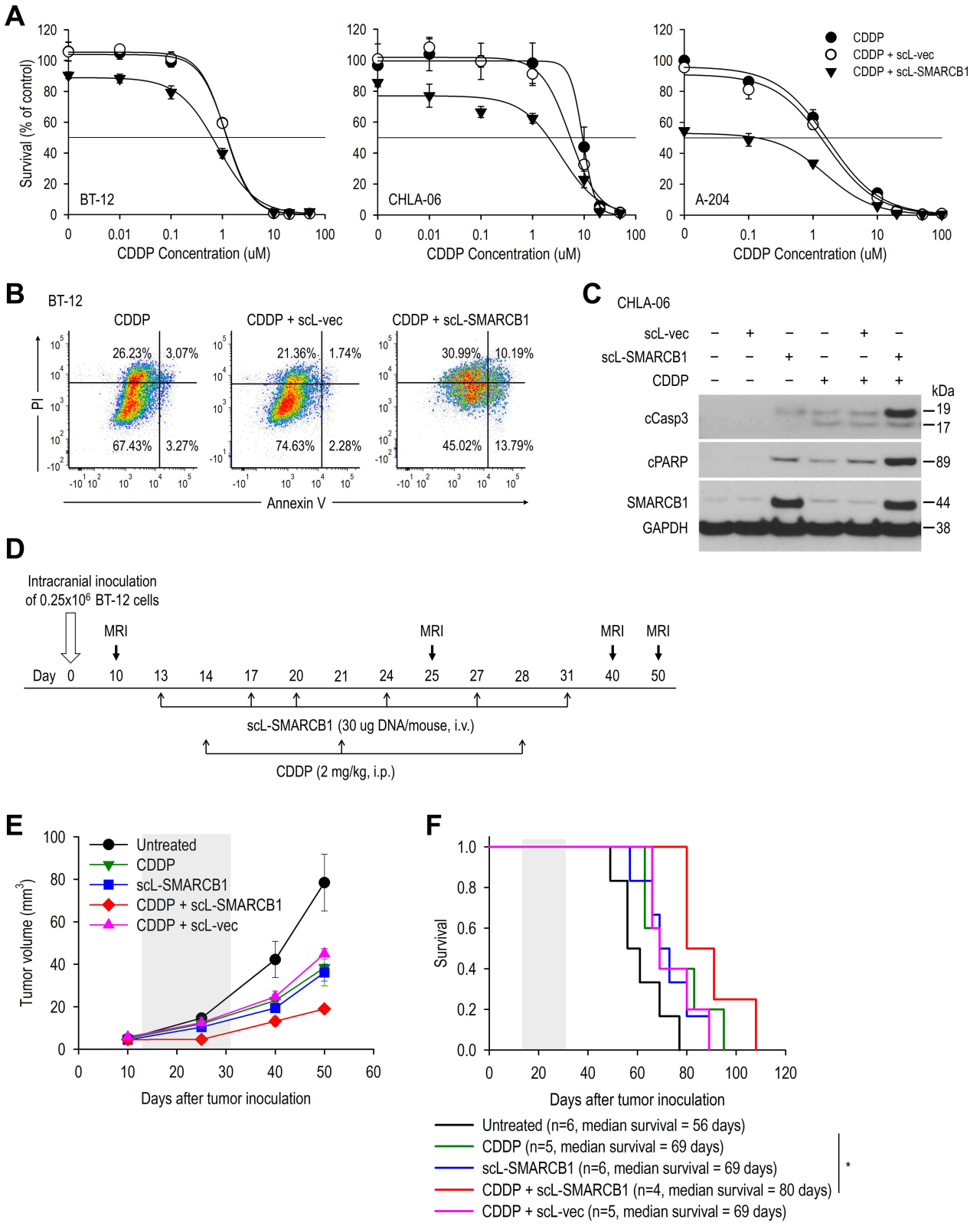

Figure 6 scL-SMARCB1 nanocomplex promotes cisplatin-induced cytotoxicity in ATRT. For in vitro study, SMARCB1-deficient ATRT (BT-12 and CHLA-06) and SMARCB1-deficient rhabdomyosarcoma (A-204) were transfected with either scL-SMARCB1 or scL-vec for 24h, followed by treatment with cisplatin at various concentration. (**A**) XTT cell viability assay at 72h after cisplatin treatment. (**B**) Annexin V/PI staining to monitor apoptosis in BT-12. Numbers in the quadrants indicate the percentage of cells in each quadrant. (**C**) Western blot analysis of SMARCB1 and apoptosis markers (cleaved PARP and cleaved Caspase3) in CHLA-06 cells. For in vivo study, athymic mice with intracranial BT-12 tumor xenografts were randomized to therapy with scL-SMARCB1 and/or cisplatin. (**D**) Treatment schedule. Mice received total 6 injections of scL-SMARCB1 (30μg/injection, twice weekly for 3 weeks) and/or total 3 injections of cisplatin (2 mg/kg, weekly for 3 weeks). (**E**) MRI-based measurement of tumor volume. Gray box indicates the treatment period. (**F**) Kaplan–Meier survival curves of mice. Log Rank test, *p<0.05. N = 4–6/group.

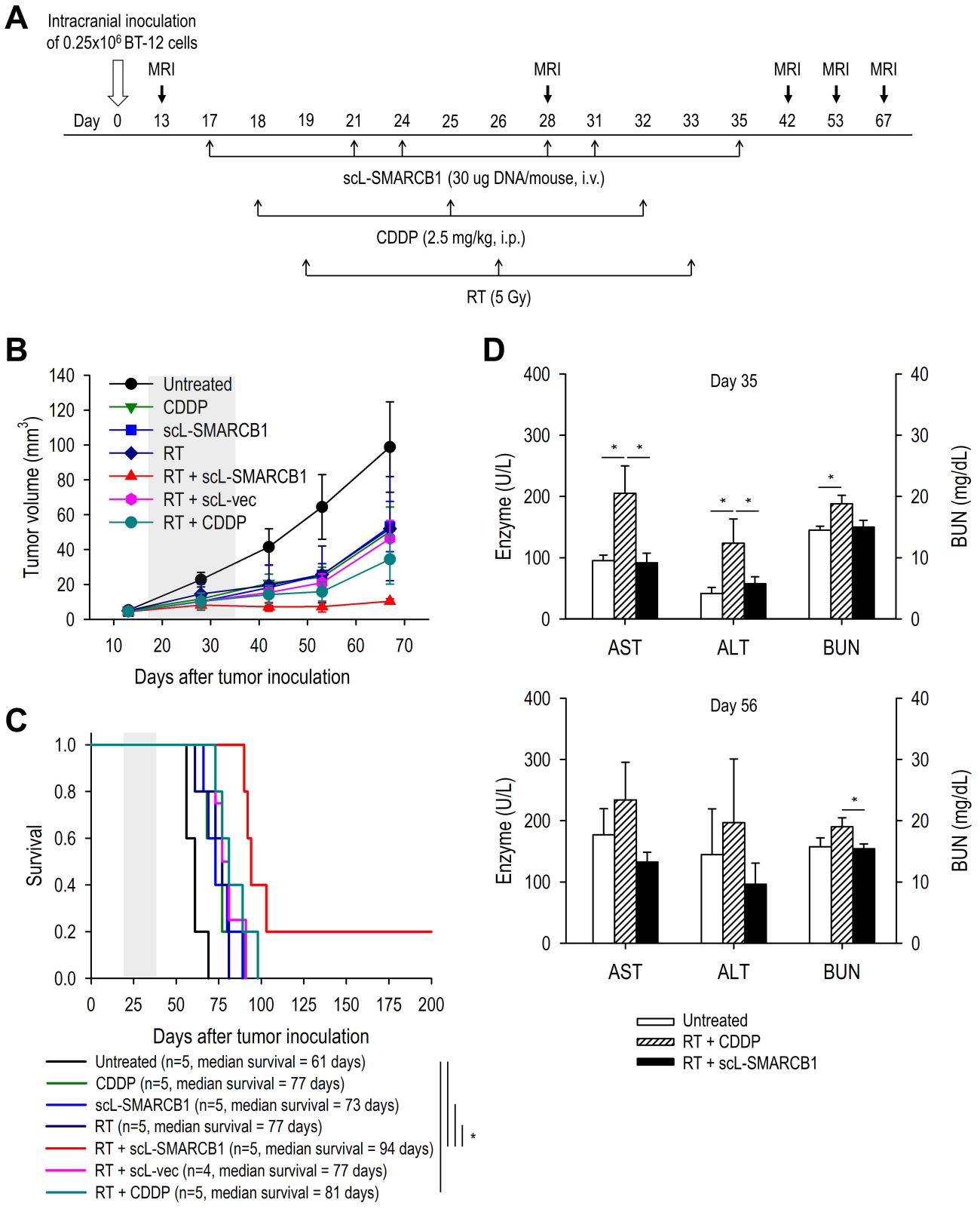

Figure 7 scL-SMARCB1 nanocomplex promotes radiation-induced cytotoxicity in ATRT. Athymic mice with intracranial BT-12 tumor xenografts were randomized to therapy with scL-SMARCB1 and/or radiation therapy. (**A**) Treatment schedule. Mice received total 6 injections of scL-SMARCB1 (30μg/injection, twice weekly for 3 weeks) and/or 3 fractions of radiation (5Gy, weekly for 3 weeks). Some animals also received total 3 injections of cisplatin (2mg/kg, weekly for 3 weeks) and/or 3 fractions of radiation (5Gy, weekly for 3 weeks). (**B**) MRI-based measurement of tumor volume. Gray box indicates the treatment period. (**C**) Kaplan–Meier survival curves of mice. Log Rank test, *p<0.05. N = 4–5/group. (**D**) Sera from tumor bearing mice receiving the indicated treatment were collected on day 35 (top panel) and day 56 (lower panel) and analyzed for levels of liver enzymes (AST and ALT) and BUN, indicators of hepatic and renal toxicity, respectively. *p<0.05. N = 4–5/group.

https://doi.org/10.2147/IJN.S458323 DovePress

in the cerebellum by MRI, treatment was initiated and tumor growth was monitored (Figure 7A). During the treatment period, significant inhibition of tumor growth was evident with the combination treatment of radiation and scL-SMARCB1 compared to untreated tumors (Figure 7B). Although radiation therapy alone and scL-SMARCB1 alone had some inhibitory effects on tumor growth, the combination of both showed a significantly stronger anti-tumor response. In contrast, combining radiation and scL-vec did not increase the antitumor response compared with radiation treatment alone. The inhibitory effect on tumor growth continued even after treatment was stopped. On day 67 (ie, 32 days after the last treatment), the average volume of tumors from mice that received both radiation and scL-SMARCB1 treatment increased by 2.3-fold from their initial size, whereas the average volume of tumors treated with radiation alone increased by 10.5-fold from their initial size. However, combining radiation and scL-vec did not improve the antitumor response (10.3-fold increase from the initial volume) compared to radiation alone. More importantly, there was a significant increase in survival when scL-SMARCB1 was combined with radiation (Figure 7C). All mice receiving radiation monotherapy succumbed to ATRT around day 81 (with a median survival time of 77 days), whereas 100% of the mice that received a combination of radiation and scL-SMARCB1 survived (with a median survival time of 94 days). In contrast, 25% of the mice receiving a combination of radiation and scL-vec survived until day 81 (with a median survival time of 77 days). Log-rank analysis demonstrated a statistically significant difference between the survival curves. These results demonstrated that 46 days after the end of treatment (ie, day 81), there was a significant difference in survival when scL-SMARCB1 was administered in combination with radiation compared to radiation treatment alone. Collectively, scL-SMARCB1 treatment enhanced radiation-induced cytotoxicity in ATRT, significantly inhibited tumor growth, and extended survival time compared to radiation treatment alone.

Interestingly, adding scL-SMARCB1 to radiation was much more effective in inhibiting ATRT growth and extending animal survival than adding cisplatin to radiation, which is similar to the currently used chemoradiation therapy in the clinic. Cisplatin treatment induces non-specific cytotoxic effects that damage normal tissues and organs, which often limit the use of drugs. Importantly, combining scL-SMARCB1 with radiation did not cause hepatotoxicity and renal injury, which were observed in mice treated with cisplatin and radiation combination therapy when the treatment was completed on day 35 (Figure 7D). Serum samples from mice treated with radiation in combination with cisplatin showed significantly elevated levels of alanine transaminase (ALT, 2.2-fold increase) and aspartate aminotransferase (AST, 3.0-fold increase), two key liver enzymes indicative of hepatocellular injury, compared to the baseline levels in the serum of untreated mice. In contrast, serum from mice treated with radiation in combination with scL-SMARCB1 showed ALT and AST levels similar to those at baseline. A significant increase in blood urea nitrogen (BUN, 1.3-fold increase from the baseline level), a clinically relevant marker of nephrotoxicity, was also observed in the serum of mice treated with radiation in combination with cisplatin, compared with serum from either untreated mice or mice treated with radiation in combination with scL-SMARCB1. A similar trend was observed in blood samples collected on day 56, confirming that fewer adverse effects were triggered when cisplatin was replaced by scL-SMARCB1 in combination with radiation. Taken together, these results indicate that combining radiation with scL-SMARCB1 is more effective and safer than conventional chemoradiotherapy. These observations suggest that scL-SMARCB1 may replace toxic chemotherapeutics for the treatment of patients with ATRT.

Discussion

Gene therapy, which involves replacement of a defective or missing gene with a functional, intact copy of that gene, is a potentially beneficial cancer treatment approach particularly over conventional chemotherapy, which often lacks selectivity and can cause non-specific toxicity.[38] To date, gene therapy for cancer has seen extremely limited clinical success due to current impediments such as intra-tumoral genetic heterogeneity, high genomic instability, and low-efficiency delivery.[5,38,39] Interestingly, ATRT, a highly aggressive and incurable pediatric brain cancer, is historically considered to be a monogenic disease.[40] Unlike other tumors, ATRT has relatively stable genome and a single genetic alteration (ie, loss of SMARCB1 gene) is the common decisive molecular defect that is almost universally found in ATRTs.[41,42] Therefore, the unique monogenic character of SMARCB1-deficient ATRTs offers an opportunity to determine the utility of our nanomedicine-based SMARCB1 gene therapy approach. As a core subunit of the chromatin remodeling complex necessary for normal eukaryotic cell function, SMARCB1 is ubiquitously expressed at high levels

throughout the body and has no known oncogenic function, thereby limiting the potential for its toxicity related to off-target effects in patients.

Our brain tumor-targeted scL-SMARCB1 nanomedicine is a novel cationic liposome encapsulating a plasmid encoding the human wild-type SMARCB1 gene. The surface of liposome is decorated with TfRscFv, which allows the nanocomplex to target brain tumor cells that overexpress TfRs with exquisite specificity and actively ferry payloads across the BBB by virtue of the elevated expression of TfRs in the cerebral endothelium via TfR-mediated transcytosis.[43] We have previously evaluated the in vivo distribution of scL nanocomplex carrying a fluorescence labeled oligonucleotide payload after a tail vein injection in tumor bearing mice.[33] Ex vivo imaging of tumors and major organs revealed a selective tumor-targeting by scL nanocomplex and much lower delivery to other major organs. However, when control nanocomplex without tumor-targeting moiety or payload itself without delivery system were injected, a significantly lower uptake of payload was seen in the tumor while significantly higher fluorescence signal was observed in liver and kidney, demonstrating a superior tumor-targeting ability of scL nanocomplex. More importantly, we have also assessed the distribution of scL nanocomplex inside the brain in non-tumor bearing BALB/c mice with an intact BBB using scL nanocomplex carrying fluorescence (Cy5-) labeled oligonucleotide through tail vein injection.[44] A strong Cy5 fluorescence signal was seen in several areas of mouse brain (eg, hippocampus, cortex, and cerebellum) as early as 6h post-injection, demonstrating that the scL nanocomplex has the ability to deliver payloads across the intact BBB after systemic administration in mice.

In our study, treatment with the scL-SMARCB1 nanocomplex successfully restored the expression of missing SMARCB1 in SMARCB1-deficient ATRT cells both in vitro and in vivo. Restoration of functional SMARCB1, a potential tumor suppressor, resulted in ATRT cell death in vitro and inhibition of tumor growth and extension of animal survival in vivo demonstrating the antitumor efficacy of scL-SMARCB1 in ATRT treatment. This antitumor effect, following the functional restoration of SMARCB1, appears to stem from the transcriptional regulation of a number of genes involved in ATRT progression. For example, overexpression of SMARCB1 significantly decreased the expression of AURKA, an oncogene, and mitotic serine/threonine-protein kinase involved in mitosis. AURKA is a direct downstream target of SMARCB1-mediated repression in malignant rhabdoid tumor cells,[45] and loss of SMARCB1 leads to aberrant expression of AURKA, which results in a weakened mitotic checkpoint, ultimately allowing ATRT to proliferate uncontrollably. Thus, suppression of AURKA by SMARCB1 restoration could be a potential mechanism by which scL-SMARCB1 treatment induces antitumor activity. In accordance with these data, AURKA inhibitors (eg, alisertib) are currently being studied as a single agent for treating ATRT in clinical trials.[46]

Although the ATRT genome is relatively stable with a low mutational burden, in addition to the characteristic alterations of SMARCB1, DNA methylation and gene expression profiling recently identified three subgroups of ATRT, ie: ATRT-MYC (MYC oncogene-driven), ATRT-SHH (activated sonic hedgehog signaling), and ATRT-TYR (active melanoma-associated genes).[14,47,48] These findings suggest that there might not be a singular molecular mechanism through which SMARCB1 universally functions as a tumor suppressor. Rather, the underlying mechanism of SMARCB1 in tumor suppression may vary depending on the ATRT subtype. In either case, the restoration of the defective or missing SMARCB1 gene is expected to reverse the effects of its inactivation. In our study, we used patient-derived cell lines (BT-12 and CHLA-06) that exhibit features that are more similar to the ATRT-MYC subgroup, with elevated expression of the MYC oncogene and activated MYC target genes. MYC, a key transcription factor, is frequently deregulated in many human cancers and has been linked to chromatin regulation through its interaction with SMARCB1.[49] Importantly, MYC and SMARCB1 bind to many common target genes and have opposing effects on gene expression in rhabdoid tumors.[49] SMARCB1 can bind to promoters of MYC target genes to inhibit DNA-binding ability of MYC resulting in an impeded MYC-driven transcriptional activity.[50] Therefore, exogenous SMARCB1 restored by scL-SMARCB1 nanocomplex could block the deregulated MYC binding to and reverse the deregulated expression of MYC target genes. In our intracranial model of ATRT-MYC tumor (BT-12), RT-qPCR analysis revealed that scL-SMARCB1 treatment resulted in SMARCB1 expression and reversed the expression of MYC-repressed tumor suppressor and MYC-activated target genes, although MYC expression remained unchanged. Linked to SMARCB1 loss, MYC represses CDK inhibitor genes including CDKN1C and CDKN2A, allowing for a proliferative advantage in ATRT cells. In our study, exogenous SMARCB1 derepressed CDKN1C and CDKN2A, and arrested the growth of ATRT cells. Conforming to our data, CDKN1C has been shown to be a downstream target of SMARCB1 and tumor suppressor gene that prevented rhabdoid tumor growth.[51] Another tumor suppressor gene CDKN2A has been shown to inhibit activity of the cyclin D1-CDK4 complex and CDK4 is MYC-activated

gene that was downregulated by scL-SMARCB1 treatment. Increased CDKN2A expression was accompanied by increased cellular senescence in BT-12 cells treated with the scL-SMARCB1 nanocomplex in vitro. Additionally, scL-SMARCB1 treatment upregulated the expression of MYC-repressed GADD45A, which has been shown to play a vital role in growth arrest[52] and to strongly inhibit AURKA kinase activity.[53] Collectively, these findings indicate that scL-SMARCB1 treatment can restore the function of SMARCB1 to fix deregulated MYC activities and inhibit unchecked growth of ATRT-MYC tumors.

Importantly, SMARCB1 loss also limits the efficacy of traditional anticancer treatments such as radiation and chemotherapy.[23,24] To date, conventional-dose chemotherapy is not effective in most ATRT patients and high-dose chemotherapy shows the potential to improve patient survival but with high toxicity and requires transfusion of autologous stem cells.[41] Moreover, unacceptable adverse effects of radiation therapy for young children with brain tumors have led a number of institutions and national groups to adopt chemotherapy-based strategies designed to avoid or delay radiation therapy, despite radiation therapy being an integral part of managing brain tumors.[54,55] Because ATRT often occurs in children under three years, radiation therapy is typically deferred, avoided, or dose reduced in order to avoid the associated neurocognitive toxicity.[41] Thus, combination therapy that combines conventional modalities with a novel therapeutic agent is predicted to be advantageous in overcoming the limited efficacy of current ATRT treatments. We studied the effects of combining scL-SMARCB1 nanocomplexes with conventional anticancer treatment modalities. SMARCB1 restoration by scL-SMARCB1 potentiated cisplatin therapy in SMARCB1-deficient ATRTs and significantly inhibited tumor growth with a survival benefit compared with cisplatin monotherapy in a mouse xenograft model. When the scL-SMARCB1 nanocomplex was added to radiation therapy, further enhanced efficacy was observed compared with radiation therapy alone, suggesting that scL-SMARCB1 could complement either cisplatin chemotherapy or radiation therapy. Notably, combining scL-SMARCB1 with radiation therapy was more effective in inhibiting ATRT growth and improving survival than combining cisplatin with radiation therapy, similar to the currently used chemoradiation treatment regimens in human patients. More importantly, combining scL-SMARCB1 with radiation therapy prevented cisplatin-induced adverse effects (ie, hepatotoxicity and renal toxicity) observed in mice treated with cisplatin plus radiation therapy. Importantly, two nanomedicines in clinical development for cancer gene therapy (ie, SGT-53 and SGT-94) based on the same tumor-targeted scL nanodelivery platform technology were well tolerated in Phase I clinical trials, suggesting the potential safety of scL-SMARCB1 treatment.[56,57] Our data suggest that scL-SMARCB1 treatment in combination with either cisplatin or radiation therapy is more effective than conventional cisplatin or radiation therapy as monotherapy, although the mechanism through which SMARCB1 potentiates either cisplatin or radiation therapy remains unclear and requires further investigation. It was recently reported that small-molecule inhibitors targeting AURKA could enhance the radiation sensitivity of ATRT cells[36] and cisplatin-induced cell death in esophageal adenocarcinoma cells,[58] suggesting that attenuation of AURKA expression by exogenous SMARCB1 restored by scL-SMARCB1 treatment could improve the efficacy of either radiotherapy or chemotherapy against SMARCB1-deficient ATRT. Moreover, functional restoration of SMARCB1 derepressed CDKN1C, a MYC-repressed tumor suppressor gene that has been shown to enhance cisplatin sensitivity via intrinsic mitochondrial apoptosis.[59]

Despite our data demonstrating a significant improvement in the survival of ATRT-bearing mice after a single cycle of treatment with a combination of scL-SMARCB1 and chemotherapy or radiotherapy, only a small fraction of mice achieved long-term survival. However, chemoradiation is usually administered over multiple cycles in the clinic. We anticipate that our combination treatment might lead to more long-term survival when administered in multiple treatment cycles; however, this hypothesis needs to be tested.

Complete loss of SMARCB1 expression has also been linked to malignant rhabdoid tumors (MRTs), one of the most aggressive childhood neoplasms of the kidneys and soft tissues that are associated with high mortality. Currently, there is no accepted standard therapy for MRT, and patients with MRT typically undergo surgical resection, chemotherapy, and radiation therapy with a very poor prognosis. Given the unique central role of SMARCB1 loss in initiating and maintaining the cancer phenotype, restoring SMARCB1 function via the scL-SMARCB1 nanocomplex offers great promise as a novel targeted therapy for MRT. In our study, treatment with the scL-SMARCB1 nanocomplex of the SMARCB1-deficient MRT cell line (A-204) showed strong antitumor effects in vitro whereas no demonstrable antitumor effects were observed in the SMARCB1-expressing MRT cell line (Hs729), demonstrating the antitumor efficacy of scL-SMARCB1 in the treatment of MRT, depending on the SMARCB1 status. Further investigation is needed to fully evaluate the antitumor efficacy of scL-SMARCB1 in MRT treatment.

Conclusion

In summary, the scL-SMARCB1 nanocomplex offers a potential new treatment option for young children and infants suffering from ATRT. Treatment with scL-SMARCB1, possibly alongside chemotherapy or radiation therapy, may offer a much more effective and safer alternative to the traditional ATRT treatment regimens.

Acknowledgement

This research was supported by the Preclinical Imaging Research Laboratory (PIRL) and Flow Cytometry & Cell Sorting Shared Resource of the Georgetown Lombardi Comprehensive Cancer Center (P30-CA051008).

Disclosure

E.H.C. is one of the inventors of the described technology, for which several patents owned by Georgetown University have been issued. The patents were licensed to SynerGene Therapeutics, Inc. for commercial development. E.H.C. has an equity interest in SynerGene Therapeutics, Inc., and E.H.C. and A.R. serve as paid scientific consultants for SynerGene Therapeutics, Inc. S.S.K. is a salaried employee of SynerGene Therapeutics, Inc. M.M. is a graduate student who was supported by a research agreement between Georgetown University and SynerGene Therapeutics, Inc. J.B.H. serves as the salaried President & CEO of SynerGene Therapeutics, Inc., and owns stock in the same. The authors report no other conflicts of interest in this work.

References

1. Siegel RL, Miller KD, Jemal A. Cancer statistics, 2018. *CA Cancer J Clin*. 2018;68(1):7–30.
2. Lau CS, Mahendraraj K, Chamberlain RS. Atypical teratoid rhabdoid tumors: a population-based clinical outcomes study involving 174 patients from the Surveillance, Epidemiology, and End Results database (1973-2010). *Cancer Manag Res*. 2015;7:301–309.
3. Ginn KF, Gajjar A. Atypical teratoid rhabdoid tumor: current therapy and future directions. *Front Oncol*. 2012;2:114.
4. Lafay-Cousin L, Hawkins C, Carret AS, et al. Central nervous system atypical teratoid rhabdoid tumours: the Canadian Paediatric Brain Tumour Consortium experience. *Eur J Cancer*. 2012;48(3):353–359.
5. Hanahan D, Weinberg RA. Hallmarks of cancer: the next generation. *Cell*. 2011;144(5):646–674.
6. Douglass EC, Valentine M, Rowe ST, et al. Malignant rhabdoid tumor: a highly malignant childhood tumor with minimal karyotypic changes. *Genes Chromosomes Cancer*. 1990;2(3):210–216.
7. Hasselblatt M, Isken S, Linge A, et al. High-resolution genomic analysis suggests the absence of recurrent genomic alterations other than SMARCB1 aberrations in atypical teratoid/rhabdoid tumors. *Genes Chromosomes Cancer*. 2013;52(2):185–190.
8. Lee RS, Stewart C, Carter SL, et al. A remarkably simple genome underlies highly malignant pediatric rhabdoid cancers. *J Clin Invest*. 2012;122 (8):2983–2988.
9. Alimova I, Pierce A, Danis E, et al. Inhibition of MYC attenuates tumor cell self-renewal and promotes senescence in SMARCB1-deficient Group 2 atypical teratoid rhabdoid tumors to suppress tumor growth in vivo. *Int j Cancer*. 2019;144(8):1983–1995.
10. Buscariollo DL, Park HS, Roberts KB, Yu JB. Survival outcomes in atypical teratoid rhabdoid tumor for patients undergoing radiotherapy in a Surveillance, Epidemiology, and End Results analysis. *Cancer*. 2012;118(17):4212–4219.
11. Biegel JA, Tan L, Zhang F, Wainwright L, Russo P, Rorke LB. Alterations of the hSNF5/INI1 gene in central nervous system atypical teratoid/ rhabdoid tumors and renal and extrarenal rhabdoid tumors. *Clini Cancer Res*. 2002;8(11):3461–3467.
12. Mathur R, Roberts CWM. SWI/SNF (BAF) Complexes: guardians of the Epigenome. *Annu Rev Canc Biol*. 2018;2:413–427.
13. Biegel JA, Allen CS, Kawasaki K, Shimizu N, Budarf ML, Bell CJ. Narrowing the critical region for a rhabdoid tumor locus in 22q11. *Genes Chromosomes Cancer*. 1996;16(2):94–105.
14. Torchia J, Golbourn B, Feng S, et al. Integrated (epi)-Genomic Analyses Identify Subgroup-Specific Therapeutic Targets in CNS Rhabdoid Tumors. *Cancer Cell*. 2016;30(6):891–908.
15. Versteege I, Sevenet N, Lange J, et al. Truncating mutations of hSNF5/INI1 in aggressive paediatric cancer. *Nature*. 1998;394:6689.
16. Chasse MH, Johnson BK, Boguslawski EA, et al. Mithramycin induces promoter reprogramming and differentiation of rhabdoid tumor. *EMBO Mol. Med.* 2021;13(2).
17. Betz BL, Strobeck MW, Reisman DN, Knudsen ES, Weissman BE. Re-expression of hSNF5/INI1/BAF47 in pediatric tumor cells leads to G1 arrest associated with induction of p16ink4a and activation of RB. *Oncogene*. 2002;21(34):5193–5203.
18. Isakoff MS, Sansam CG, Tamayo P, et al. Inactivation of the Snf5 tumor suppressor stimulates cell cycle progression and cooperates with p53 loss in oncogenic transformation. *Proc Natl Acad Sci U S A*. 2005;102(49):17745–17750.
19. Lee D, Kim JW, Seo T, Hwang SG, Choi EJ, Choe J. SWI/SNF complex interacts with tumor suppressor p53 and is necessary for the activation of p53-mediated transcription. *J Biol Chem*. 2002;277(25):22330–22337.
20. Lee S, Cimica V, Ramachandra N, Zagzag D, Kalpana GV. Aurora A is a repressed effector target of the chromatin remodeling protein INI1/hSNF5 required for rhabdoid tumor cell survival. *Cancer Res*. 2011;71(9):3225–3235.
21. Oruetxebarria I, Venturini F, Kekarainen T, et al. P16INK4a is required for hSNF5 chromatin remodeler-induced cellular senescence in malignant rhabdoid tumor cells. *J Biol Chem*. 2004;279(5):3807–3816.
22. Versteege I, Medjkane S, Rouillard D, Delattre O. A key role of the hSNF5/INI1 tumour suppressor in the control of the G1-S transition of the cell cycle. *Oncogene*. 2002;21(42):6403–6412.

23. Fruhwald MC, Biegel JA, Bourdeaut F, Roberts CW, Chi SN. Atypical teratoid/rhabdoid tumors-current concepts, advances in biology, and potential future therapies. *Neuro-Oncology*. 2016;18(6):764–778.
24. Lee YE, Choi SA, Kwack PA, et al. Repositioning disulfiram as a radiosensitizer against atypical teratoid/rhabdoid tumor. *Neuro-Oncology*. 2017;19(8):1079–1087.
25. Xu L, Huang CC, Huang W, et al. Systemic tumor-targeted gene delivery by anti-transferrin receptor scFv-immunoliposomes. *Mol Cancer Ther*. 2002;1(5):337–346.
26. Kim SS, Rait A, Kim E, et al. A nanoparticle carrying the p53 gene targets tumors including cancer stem cells, sensitizes glioblastoma to chemotherapy and improves survival. *ACS nano*. 2014;8(6):5494–5514.
27. Kim SS, Harford JB, Pirollo KF, Chang EH. Effective treatment of glioblastoma requires crossing the blood-brain barrier and targeting tumors including cancer stem cells: the promise of nanomedicine. *Biochem Biophys Res Commun*. 2015;468(3):485–489.
28. Kim SS, Rait A, Kim E, DeMarco J, Pirollo KF, Chang EH. Encapsulation of temozolomide in a tumor-targeting nanocomplex enhances anti-cancer efficacy and reduces toxicity in a mouse model of glioblastoma. *Cancer Lett*. 2015;369(1):250–258.
29. Xu L, Pirollo KF, Tang WH, Rait A, Chang EH. Transferrin-liposome-mediated systemic p53 gene therapy in combination with radiation results in regression of human head and neck cancer xenografts. *Hum Gene Ther*. 1999;10(18):2941–2952.
30. Daniels TR, Bernabeu E, Rodriguez JA, et al. The transferrin receptor and the targeted delivery of therapeutic agents against cancer. *Biochim Biophys Acta*. 2012;1820(3):291–317.
31. Prior R, Reifenberger G, Wechsler W. Transferrin receptor expression in tumours of the human nervous system: relation to tumour type, grading and tumour growth fraction. *Virchows Arch a Pathol Anat Histopathol*. 1990;416(6):491–496.
32. Xu L, Tang WH, Huang CC, et al. Systemic p53 gene therapy of cancer with immunolipoplexes targeted by anti-transferrin receptor scFv. *Mol Med*. 2001;7(10):723–734.
33. Kim SS, Rait A, Rubab F, et al. The clinical potential of targeted nanomedicine: delivering to cancer stem-like cells. *Mol Ther*. 2014;22 (2):278–291.
34. GeneCards: The Human Gene Database [homepage on the Internet]. Rehovot, Israel: Weizmann Institute of Science; 2024. Available from: https://www.genecards.org/cgi-bin/carddisp.pl?gene=SMARCB1. Accessed May 20, 2024.
35. Morozov A, Lee SJ, Zhang ZK, Cimica V, Zagzag D, Kalpana GV. INI1 induces interferon signaling and spindle checkpoint in rhabdoid tumors. *Clini Cancer Res*. 2007;13(16):4721–4730.
36. Venkataraman S, Alimova I, Tello T, et al. Targeting Aurora Kinase A enhances radiation sensitivity of atypical teratoid rhabdoid tumor cells. *J Neurooncol*. 2012;107(3):517–526.
37. Major K, Daggubati LC, Mau C, Zacharia B, Glantz M, Pu C. Sellar Atypical Teratoid/Rhabdoid Tumors (AT/RT): a Systematic Review and Case Illustration. *Cureus*. 2022;14(7).
38. Das SK, Menezes ME, Bhatia S, et al. Gene Therapies for Cancer: strategies, Challenges and Successes. *J Cell Physiol*. 2015;230(2):259–271.
39. van Haasteren J, Li J, Scheideler OJ, Murthy N, Schaffer DV. The delivery challenge: fulfilling the promise of therapeutic genome editing. *Nat Biotechnol*. 2020;38(7):845–855.
40. Hoffman LM, Richardson EA, Ho B, et al. Advancing biology-based therapeutic approaches for atypical teratoid rhabdoid tumors. *Neuro-Oncology*. 2020;22(7):944–954.
41. Richardson EA, Ho B, Huang A. Atypical Teratoid Rhabdoid Tumour: from Tumours to Therapies. *J Korean Neurosurg Soc*. 2018;61(3):302–311.
42. Thakur S, Ruan Y, Zhang C, Lun X, Jayanthan A, Narendran A. Human SNF5 arming of double-deleted vaccinia virus shows oncolytic and cytostatic activity against central nervous system atypical teratoid/rhabdoid tumor cells. *Cancer Gene Ther*. 2021;28(7–8).
43. Pulgar VM. Transcytosis to Cross the Blood Brain Barrier, New Advancements and Challenges. *Front Neurosci*. 2018;12:1019.
44. Kim SS, Rait A, Garrido-Sanabria ER, Pirollo KF, Harford JB, Chang EH. Nanotherapeutics for Gene Modulation that Prevents Apoptosis in the Brain and Fatal Neuroinflammation. *Mol Ther*. 2018;26(1):84–94.
45. Kohashi K, Oda Y. Oncogenic roles of SMARCB1/INI1 and its deficient tumors. *Cancer Sci*. 2017;108(4):547–552.
46. Upadhyaya SA, Campagne O, Billups CA, et al. Phase II study of alisertib as a single agent for treating recurrent or progressive atypical teratoid/rhabdoid tumor. *Neuro-Oncology*. 2023;25(2):386–397.
47. Ho B, Johann PD, Grabovska Y, et al. Molecular subgrouping of atypical teratoid/rhabdoid tumors-A reinvestigation and current consensus. *Neuro-Oncology*. 2020;22(5):613–624.
48. Johann PD, Erkek S, Zapatka M, et al. Atypical Teratoid/Rhabdoid Tumors Are Comprised of Three Epigenetic Subgroups with Distinct Enhancer Landscapes. *Cancer Cell*. 2016;29(3):379–393.
49. Stojanova A, Tu WB, Ponzielli R, et al. MYC interaction with the tumor suppressive SWI/SNF complex member INI1 regulates transcription and cellular transformation. *Cell Cycle*. 2016;15(13):1693–1705.
50. Weissmiller AM, Wang J, Lorey SL, et al. Inhibition of MYC by the SMARCB1 tumor suppressor. *Nat Commun*. 2019;10(1):2014.
51. Algar EM, Muscat A, Dagar V, et al. Imprinted CDKN1C is a tumor suppressor in rhabdoid tumor and activated by restoration of SMARCB1 and histone deacetylase inhibitors. *PLoS One*. 2009;4(2).
52. Marhin WW, Chen S, Facchini LM, Fornace AJ, Penn LZ. Myc represses the growth arrest gene gadd45. *Oncogene*. 1997;14(23):2825–2834.
53. Shao S, Wang Y, Jin S, et al. Gadd45a interacts with Aurora-A and inhibits its kinase activity. *J Biol Chem*. 2006;281(39):28943–28950.
54. Duffner PK, Horowitz ME, Krischer JP, et al. Postoperative chemotherapy and delayed radiation in children less than three years of age with malignant brain tumors. *N Engl J Med*. 1993;328(24):1725–1731.
55. Grill J, Sainte-Rose C, Jouvet A, et al. Treatment of medulloblastoma with postoperative chemotherapy alone: an SFOP prospective trial in young children. *Lancet Oncol*. 2005;6(8):573–580.
56. Senzer N, Nemunaitis J, Nemunaitis D, et al. Phase I study of a systemically delivered p53 nanoparticle in advanced solid tumors. *Mol Ther*. 2013;21(5):1096–1103.
57. Siefker-Radtke A, Zhang XQ, Guo CC, et al. A Phase l Study of a Tumor-targeted Systemic Nanodelivery System, SGT-94, in Genitourinary Cancers. *Mol Ther*. 2016;24(8):1484–1491.

58. Sehdev V, Peng D, Soutto M, et al. The Aurora kinase A inhibitor MLN8237 enhances cisplatin-induced cell death in esophageal adenocarcinoma cells. *Mol Cancer Ther*. 2012;11(3):763–774.
59. Vlachos P, Nyman U, Hajji N, Joseph B. The cell cycle inhibitor p57(Kip2) promotes cell death via the mitochondrial apoptotic pathway. *Cell Death Differ*. 2007;14(8):1497–1507.

International Journal of Nanomedicine Dovepress

Publish your work in this journal

The International Journal of Nanomedicine is an international, peer-reviewed journal focusing on the application of nanotechnology in diagnostics, therapeutics, and drug delivery systems throughout the biomedical field. This journal is indexed on PubMed Central, MedLine, CAS, SciSearch®, Current Contents®/Clinical Medicine, Journal Citation Reports/Science Edition, EMBase, Scopus and the Elsevier Bibliographic databases. The manuscript management system is completely online and includes a very quick and fair peer-review system, which is all easy to use. Visit http://www.dovepress.com/testimonials.php to read real quotes from published authors.

Submit your manuscript here: https://www.dovepress.com/international-journal-of-nanomedicine-journal